BioMetals (2005) 18:449–466
DOI 10.1007/s10534-005-4303-8

Structural analysis of divalent metals binding to the *Bacillus subtilis* response regulator Spo0F: the possibility for *in vitro* metalloregulation in the initiation of sporulation

Douglas J. Kojetin[1], Richele J. Thompson[1], Linda M. Benson[2], Stephen Naylor[2,6], Jenora Waterman[3], Keith G. Davies[4], Charles H. Opperman[3], Keith Stephenson[5,7], James A. Hoch[5] & John Cavanagh[1,*]

[1]*Department of Molecular and Structural Biochemistry, North Carolina State University, Raleigh, NC, USA;* [2]*Biomedical Mass Spectrometry and Functional Proteomics Facility, Department of Biochemistry and Molecular Biology, Mayo Clinic/Foundation, Rochester, MN, 55905, USA;* [3]*Department of Plant Pathology, Center for the Biology of Nematode Parasitism, North Carolina State University, Raleigh, NC, 27695, USA;* [4]*Nematode Interaction Unit, Rothamsted Research Limited, Harpenden, Herts, AL52JQ, UK;* [5]*Division of Cellular Biology, Department of Molecular and Experimental Medicine, The Scripps Research Institute, La Jolla, CA, 92037, USA;* [6]*Division of Biological Engineering, Room 56-738, MIT, Cambridge, MA, 02139, USA;* [7]*School of Biochemistry and Microbiology, University of Leeds, Leeds, LS2 9JT, UK; *Author for correspondence (Tel: +1-919-513-4349; Fax: +1-919-515-2047; E-mail: john_cavanagh@ncsu.edu)*

Received 8 March 2005; accepted 22 March 2005

Key words: metal binding, NMR spectroscopy, response regulator, sporulation, two-component signal transduction

Abstract

The presence of a divalent metal ion in a negatively charged aspartic acid pocket is essential for phosphorylation of response regulator proteins. Here, we present metal binding studies of the *Bacillus subtilis* response regulator Spo0F using NMR and μESI-MS. NMR studies show that the divalent metals Ca^{2+}, Mg^{2+} and Mn^{2+} primarily bind, as expected, in the Asp pocket phosphorylation site. However, identical studies with Cu^{2+} show distinct binding effects in three specific locations: (i) the Asp pocket, (ii) a grouping of charged residues at a site opposite of the Asp pocket, and (iii) on the β4-α4 loop and the β5/α5 interface, particularly around and including H101. μESI-MS studies stoichiometrically confirm the NMR studies and demonstrate that most divalent metal ions bind to Spo0F primarily in a 1:1 ratio. Again, in the case of Cu^{2+}, multiple metal-bound species are observed. Subsequent experiments reveal that Mg^{2+} supports phosphotransfer between KinA and Spo0F, while Cu^{2+} fails to support KinA phosphotransfer. Additionally, the presence of Cu^{2+} at non-lethal concentrations in sporulation media for *B. subtilis* and the related organism *Pasteuria penetrans* was found to inhibit spore formation while continuing to permit vegetative growth. Depending on the type of divalent metal ion present, *in vitro* phosphorylation of Spo0F by its cognate kinase KinA can be inhibited.

Introduction

The transfer of a phosphoryl group from one protein to another forms the basis of signal propagation in many cellular regulatory pathways (West & Stock 2001). In order to sense and adapt to their environment, bacteria make use of a ubiquitous signal transduction module known as the 'two-component system'. The role of a two-component system is to transfer a phosphoryl group from a sensor kinase to a response regulator protein (Burbulys *et al.* 1991; Mizuno 1998). The

initiation of sporulation in *B. subtilis* is controlled by a specialized version of the two-component system, the phosphorelay, which has been extensively studied (Burbulys *et al.* 1991). In the phosphorelay, a phosphoryl group is first transferred from one of five sensor kinases to the response regulator Spo0F. Subsequently, Spo0F transfers the phosphoryl group to the phosphotransferase Spo0B, which finally delivers it to the response regulator/transcription factor Spo0A. Phosphorylation of Spo0A enhances the activation and repression of approximately 500 stationary phase and sporulation genes (Fawcett *et al.* 2000).

Like all known response regulators, Spo0F requires a divalent metal ion to be present in the conserved aspartic acid pocket in order to become phosphorylated (Grimshaw *et al.* 1998). The presence of the cationic positive charge ensures that the negative character of the pocket is offset, thereby allowing the negative phosphate moiety to approach and bind. Phosphorylation of Spo0F has been shown to be magnesium dependent (Zapf *et al.* 1996). Previous biochemical and structural analyses of Spo0F have identified regions affected by magnesium binding, and regions of importance for protein–kinase, protein–phosphatase and protein–phosphotransferase interactions (Feher *et al.* 1995, 1997, 1998; Tzeng & Hoch 1997; Tzeng *et al.* 1998; Jiang *et al.* 1999; Zapf *et al.* 2000). Feher *et al.* observed that a single magnesium ion binds to Spo0F in the Asp pocket, which also has been demonstrated for other metals such as Ca^{2+} and Mn^{2+} (Madhusudan *et al.* 1996; Mukhopadhyay *et al.* 2004). Interestingly, at much higher concentrations, a second Mg^{2+} was seen to bind very weakly and cause perturbations in the vicinity of the β4-α4 loop (Feher *et al.* 1995). Because of the concentration required to elicit this structural perturbation, this site is extremely unlikely to be populated by magnesium ions *in vivo*. However, Feher *et al.* suggest that this region may bind a different metal cation. More recently, it has been suggested that metals other than the commonly accepted Mg^{2+} may play a role in the initiation of sporulation in *B. subtilis* (Mukhopadhyay *et al.* 2004). In this study we report a comprehensive analysis of the effects of four divalent metals, Ca^{2+}, Cu^{2+}, Mg^{2+} and Mn^{2+} on the structure and function of Spo0F from *B. subtilis* using a complementary NMR spectroscopy and microelectrospray ionization mass spectrometry (μESI-MS) approach.

Materials and methods

Preparation of protein samples

Unlabeled and ^{15}N labeled Spo0F samples were expressed and purified as previously described (Feher *et al.* 1995; Zapf *et al.* 1996; Tzeng & Hoch 1997). KinA (10 μM) was phosphorylated in EPPS buffer (50 mM K-EPPS (4-(2-hydroxyethyl)-1-piperazinepropanesulfonic acid pH 8.5, 500 μM $MgCl_2$, 100 μM EDTA and 5% (v/v) glycerol) in a final volume of 1 ml. The reaction was initiated by the addition of 100 μCi of [γ-^{32}P]ATP diluted to a final concentration of 200 μM with unlabeled ATP. The reaction proceeded at 25 °C for 20 min and unincorporated [γ-^{32}P]ATP and the phosphorylation buffer (including Mg^{2+}) were removed by dialysis against 25 mM Tris–HCl pH 8.0, 5% (v/v) glycerol in a Slide-a-lyzer cassette (Pierce, 10,000 MWCO) at 4 °C. Dialysis was continued with frequent buffer changes until radioactive counts were no longer detectable in the dialysis buffer. KinA~P was concentrated using Microcon-30 columns and concentration determined using the Bio-Rad protein assay. The removal of [γ-^{32}P]ATP from the sample was confirmed using PEI Cellulose thin layer chromatography with 0.75 M KH_2PO_4 pH 3.75 as the solvent.

NMR ^{1}H–^{15}N HSQC metal titrations

^{15}N labeled Spo0F samples used for NMR data collection contained approximately 1 mM protein, were approximately 99% pure, and were dialyzed into a buffer of 25 mM Tris pH 6.9, 50 mM KCl, and 0.02% NaN_3. Metal titrations were performed using chloride salts and monitored by means of ^{1}H–^{15}N HSQC experiments (Bax *et al.* 1990; Cavanagh *et al.* 1996). NMR experiments were run at 300 K on either a Bruker DRX 500 equipped with 3 radiofrequency channels and a triple axis pulsed field gradient triple resonance probe or on a Varian Inova 600 spectrometer equipped with 4 radiofrequency channels and a single axis pulsed field gradient triple resonance probe. Spectral widths – DRX 500: ^{1}H, 7000 Hz; ^{15}N, 1343 Hz;

Inova 600: ^{1}H, 8000 Hz; ^{15}N, 1900 Hz. The carrier was placed on the water resonance in the ^{1}H dimension and at 118.5 ppm in the ^{15}N dimension. 1024×128 complex points were recorded in the ^{1}H dimension and ^{15}N dimensions, respectively. Prior to zero filling once during processing in each dimension, the weighting functions (i) line broadening of 3 Hz in the acquisition dimension and (ii) a 60° degree shifted sine-bell in the indirect dimension were performed. Data were referenced to previously published chemical shifts for Spo0F (Feher *et al.* 1997), processed with NMRPipe (Delaglio *et al.* 1995) and analyzed with NMRView (Johnson & Blevins 1994).

Concentration ranges of metal ions during the titrations were as follows: Ca^{2+} 0–151 mM; Cu^{2+} 0–1.169 mM; Mg^{2+} 0–147 mM; Mn^{2+} 0–433 μM. Diamagnetic metal concentration ranges were chosen to be similar to the protein:metal ratios from a previous Mg^{2+} titration (Feher *et al.* 1995). Titrations of diamagnetic metals were analyzed by measuring changes in ^{1}H–^{15}N backbone chemical shifts as a function of metal concentration using the minimum chemical shift difference method (Farmer *et al.* 1996):

$$\Delta\delta_{\min} = [\Delta\delta(^{1}\mathrm{HN})^{2} + (0.1 \times \Delta\delta^{15}\mathrm{N})^{2}]^{0.5}$$

Titrations of paramagnetic metals were analyzed by measuring ^{1}H–^{15}N chemical shift peak intensity and line broadening as a function of metal concentration and normalized based on the individual intensities for each peak in base spectrum with no metal. The following trends in chemical shift changes and line broadening were considered when plotting titration trends onto the structure of Spo0F: $Mg^{2+}, \Delta\delta_{\min} > 0.2$ ppm; Ca^{2+}, $\Delta\delta_{\min} > 0.23$ ppm; Mn^{2+} and Cu^{2+}, residues that experience the most significant decreases in slope and intensity as a function of metal concentration. The colors and symbols used in the graphical plots are respective of sequence position, with the exception of residues in the paramagnetic titrations that display relatively little change in intensity/line broadening, which are shown with blue dotted lines. Distances of residues with reference to Asp pocket were measured between the HN atom of the residue of interest and CG atom of D11. Graphical analysis was performed using MATLAB (The MathWorks, Inc, Natick, MA) and structural images were prepared with PyMOL (DeLano Scientific).

μESI-MS metal titrations

^{15}N-labeled Spo0F (1.7 mg/ml) was exchanged from a buffer of 10 mM KH_2PO_4, 50 mM KCl, 0.02% NaN_3, pH 6.9 and into 20 mM NH_4OAc using ChromaSpin^{TM} columns (Clontech Laboratories, Palo Alto, CA). Protein was diluted into a 20 μl to a final concentration of 6 μM. Protein, metal, and buffer solutions were combined in 20 μl solution volumes and incubated 10–15 min at room temperature prior to direct infusion into the ESI source. Metal acetate salts were prepared in H_2O at a concentration of 10 mM and titrated resulting in final buffer solutions (pH 6.9) with metal concentrations of 0, 125, 250, 375, 500, or 1000 μM. Protein:metal ratios used were (i) similar to ratios used in this and previous Mg^{2+}NMR titrations, and (ii) above the previously reported 20 ± 5 mM K_d for Mg^{2+} of Spo0F (Feher *et al.* 1995).

Mass spectrometry analyses were performed on a MAT 900 mass spectrometer (Finnigan-MAT, Bremen, Germany) of electrostatic-magnetic (EB) geometry. ESI measurements were performed in positive mode. Protein solutions were introduced into a modified Finnigan ESI source via a 50 mm i.d. fused silica emitter using a 10-ml syringe and a Harvard Apparatus Model 22 syringe pump (South Natick, MA) at a flow rate of 0.2 μl/min. SF_6 was introduced through the auxiliary port at 1.6 l/min in order to prevent source corona discharge and enhance the signal-to-noise ratio. The ESI source voltage was 2.6 kV, with a capillary temperature of 60 °C. The magnetic was scanned from m/z 1000–6000 at a rate of 5 s/decade. A position and time resolved ion counter (PATRIC) was used for ion detection. Multiple scans were summed and analyzed using the Finnigan MAT software (Bioworks 1.0). Multiply charged species were transformed onto a M_R scale using algorithms supplied with the instrument data system.

Phosphotransfer from KinA∼P to Spo0F

Phosphotransfer was carried out in 50 mM EPPS pH 8.5, 5% (v/v) glycerol. KinA∼P (1 μM) was mixed with Spo0F (6 μM) that had been preincubated with $MgCl_2$ or $CuCl_2$ at the concentrations of 0, 200, 400 or 1000 μM. The phosphotransfer reaction was allowed to proceed at 25 °C for 15 min. Reactions were stopped by the addition of

0.2 volumes of 5 × SDS-PAGE sample buffer (250 mM Tris–HCl pH 6.8, 10% (v/v) glycerol, 1% (w/v) SDS, 280 mM β-mercaptoethanol and 0.01% bromophenol blue) followed by flash freezing in a dry ice/ethanol bath. Identical reactions were carried out in the absence of Spo0F to determine the stability of KinA~P in the presence of the aforementioned cations. Radiolabeled KinA~P and Spo0F~P were separated with 15% (w/v) SDS-PAGE gels using the tricine buffer system. The amount of KinA~P and Spo0F~P was quantified by phosphor-imaging (Molecular Dynamics Phosphorimager SF) and analyzed with the associated software (ImageQuant, Amersham Biosciences).

Sporulation experiments

B. subtilis (strain from American Type Culture collection 23857) sporulation was induced by plating 50 μl of Potato Extract Medium liquid culture on solid Difco sporulation medium (Schaeffer *et al.* 1965) at 32 °C without $CuCl_2$ or increasing amounts of $CuCl_2$ as shown in Table 1. Degree of cell growth and sporulation was detected by visual inspection.

In vitro P. penetrans (Gainesville, Fl Isolate; Pasteuria Biosciences) cultures were maintained in an appropriate medium (Pasteuria Biosciences) (Gerber *et al.* 2003), with or without 3.89×10^{-3} M $CuSO_4$ at 30 °C (copper dependence experiments), or with or without 3.89×10^{-3} M $CuSO_4$, 1.11×10^{-3} M $ZnSO_4$ and 3.22×10^{-3} M EDTA at 30 °C (varied composition experiments). The standard medium contains 3.89×10^{-3} M Cu^{2+}, 1.11×10^{-3} M Zn^{2+} and 3.22×10^{-3} M EDTA. Images were taken with a Zeiss Axiovert (inverted) light microscope at 320 × and spore count taken by visual inspection. Cultures were approximately 14 days old.

Table 1. Summary of the effect of copper on *B. subtilis* growth and spore formation.

Experiment #	Cu^{2+} added (M)	Cell growth	Spore formation
0	0	Yes	Yes
1	9.97×10^{-5}	Yes	No
2	5.01×10^{-4}	Yes	No
3	1.47×10^{-4}	Little	No
4	2.93×10^{-3}	No	N/A
5	9.97×10^{-3}	No	N/A
6	5.00×10^{-3}	No	N/A
7	1.00×10^{-1}	No	N/A

Results

Metal binding to B. subtilis Spo0F studied by NMR

Metal ion binding to *B. subtilis* Spo0F was monitored using ^{1}H–^{15}N HSQC NMR experiments (Bax *et al.* 1990; Cavanagh *et al.* 1996). This approach enables the site of metal ion binding to be determined by monitoring changes in chemical shift and/or line broadening of previously assigned resonances in the protein spectrum during a titration. For diamagnetic metal binding (Mg^{2+} and Ca^{2+}), chemical shift changes and minor line broadening effects due to conformational exchange are predominantly used to monitor structural perturbations caused by metal ion binding. For the most part, large chemical shift changes identify regions that are directly involved in metal ion binding. In some cases there may be a few effects for resonances distant from the binding site due to global conformational alterations associated with metal binding. However, our knowledge of the structure of Spo0F in both its unphosphorylated (Feher *et al.* 1995, 1997; Madhusudan *et al.* 1997), metal-bound (Madhusudan *et al.* 1996; Mukhopadhyay *et al.* 2004) and phosphorylated/BeF_3-active (Gardino *et al.* 2003) states allows us to straightforwardly discriminate between effects in the spectra due to direct metal ion binding or as a result of conformational changes removed from the binding site. In addition, this approach allows us to identify multiple ions binding with different affinities. A diamagnetic metal ion that binds with a high affinity will elicit resonance movement, or perturbation, at lower metal concentrations than for a metal ion binding with lower affinity. With these points in mind, we can unambiguously determine the specific locations of diamagnetic metal ion binding.

For paramagnetic metals (Cu^{2+} and Mn^{2+}), titrations were followed by carefully monitoring peak intensity changes and line broadening. Differential line broadening in the ^{1}H–^{15}N HSQC spectra, due to relaxation processes involving an unpaired electron from the metal ion, can be used

to easily localize sites of paramagnetic ion binding. It is well known that the linewidths of all peaks in the ^{1}H–^{15}N HSQC spectrum broaden slightly to some degree as the concentration of the paramagnetic ion increases (Bertini & Luchinat 1998). However, those residues that specifically and locally interact with the metal ion will significantly broaden and usually disappear at an earlier point in the titration. Consequently, it is possible to identify specific sites of metal ion interaction by observing differential line broadening in the ^{1}H–^{15}N HSQC spectrum as the titration progresses.

Figure 1 illustrates characteristic examples of the changes discussed above seen in the ^{1}H–^{15}N HSQC of *B. subtilis* Spo0F spectra as a consequence of both diamagnetic and paramagnetic metal titrations. Figure 1a, b shows an overlay of ^{1}H–^{15}N HSQC spectra during the full course of the Mg^{2+} and Ca^{2+} titrations. Figure 1c, d and e, f shows spectra of the Mn^{2+} and Cu^{2+} titrations at the beginning and at a later point where residues known to coordinate a divalent metal ion in the Asp pocket display binding effects (Lukat *et al.* 1990; Feher *et al.* 1995; Madhusudan *et al.* 1996; Mukhopadhyay *et al.* 2004). The residue highlighted in Figure 1 is D11, a divalent metal coordinating residue found within the Asp pocket. D11 should be affected as a result of metal titration since previous studies have shown that response regulators, such as Spo0F, bind divalent metals in the Asp pocket.

As expected and as previously shown (Feher *et al.* 1995), titration of the divalent metal Mg^{2+} results in a significant chemical shift perturbation for residue D11 (Figure 1a – green box). Other residues shown in Figure 1a that are more distant from the metal coordinate site in the Asp pocket, such as V51 (approx. 18 Å) and L52 (approx. 14 Å), do not experience notable chemical shift perturbations as a result of Mg^{2+} titration. Titration of diamagnetic Ca^{2+} (Figure 1b – yellow box) shows trends similar to the Mg^{2+} titration.

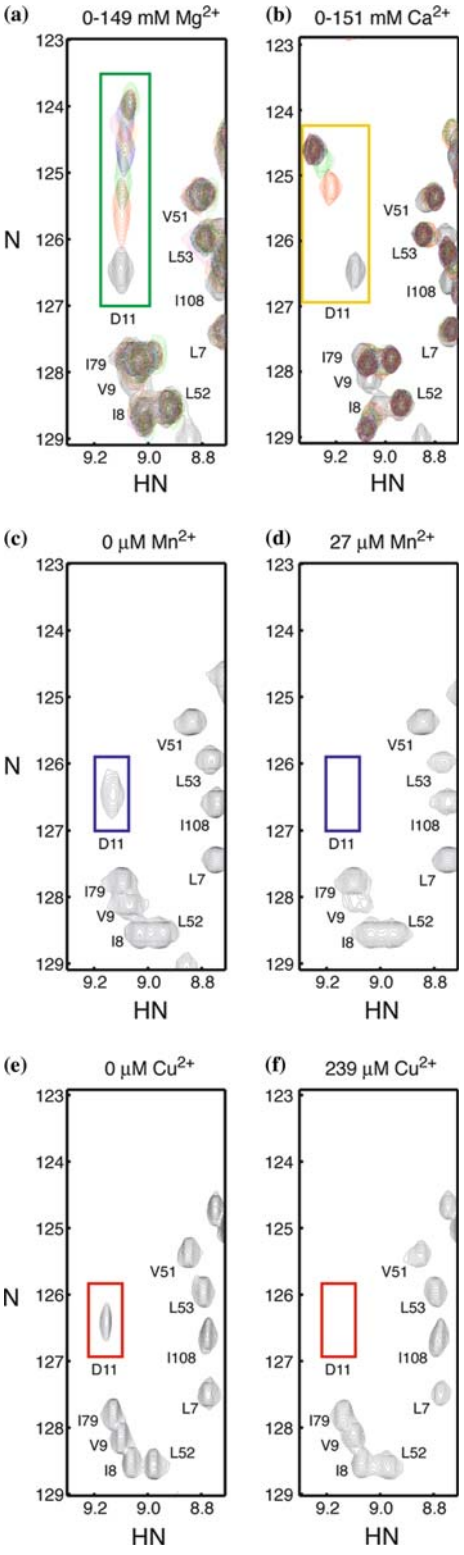

Figure 1. Changes observed in regions of ^{1}H–^{15}N HSQC spectra of *B. subtilis* Spo0F as a consequence of metal titration. Perturbations caused by titration of (a) Mg^{2+} and (b) Ca^{2+} and paramagnetic-induced line broadening caused by (c, d) Mn^{2+} and (e, f) Cu^{2+}. Residue D11 is boxed for emphasis (Mg^{2+} green; Ca^{2+} yellow; Mn^{2+} blue; Cu^{2+} red) and is discussed in detail in the text.

D11 experiences a notable chemical shift perturbation, while other residues do not experience notable changes, such as V51 and L52. Another residue near the Asp pocket, I8 (approx. 13 Å), shows a slightly higher perturbation in the Ca^{2+} titration compared to the Mg^{2+} titration although the changes are minor in comparison to D11. This may be a consequence of the higher binding affinity of Ca^{2+} vs. Mg^{2+} for Spo0F and a possible deep pocket binding effect (Mukhopadhyay *et al*. 2004). Titration of the paramagnetic metal Mn^{2+} causes severe line broadening for the direct metal binding residue D11 to the point where its peak 'disappears' (Figure 1c, d – blue box), while a residue near the metal coordinate site in the Asp pocket, V9 (approx. 10 Å), shows only a moderate line broadening as a result of metal titration. As in the case of Mg^{2+} and Ca^{2+}, residues that are distant from the metal coordination site in Asp pocket, such as V51 and L52, display only nominal effects as a result of Mn^{2+} titration. Lastly, titration of Cu^{2+} also causes severe line broadening in the case of D11 (Figure 1e, f – red box). However, unlike the Mn^{2+} titration where V9 was moderately affected, Cu^{2+} causes only minimal effects to this residue, as well as to V51 and L52.

There are notable differences between the paramagnetic-induced line broadening of Mn^{2+} and Cu^{2+}. These differences are apparent when comparing the concentration ranges that result in line broadening effects, in the initial slopes of the titration curves, as well as in the overall degree to which metal-interacting atoms are affected. For example, the peak corresponding to D11 disappears at ~10-fold less concentration of Mn^{2+} (Figure 1c, d) than for the same peak in the Cu^{2+} titration (Figure 1e, f). This differential broadening is not likely due to differences in affinity, but rather an NMR phenomenon that is a result of the different electronic correlation times, τ_s, for these paramagnetic species (Bertini & Luchinat 1998). Mn^{2+} and Cu^{2+} have τ_s values of 10^{-8} s and 10^{-9} s, respectively. The 10-fold differences in local linewidth effects observed between the Mn^{2+} and Cu^{2+} titration data can be attributed directly to the factor of 10 difference in τ_s between these moieties (Bertini & Luchinat 1998). It should be noted that the experiments utilizing paramagnetic ions could not be used to evaluate relative binding affinities between different paramagnetic metals. However, depending on the electronic correlation time, slopes of resonance decay in a single paramagnetic ion titration can be used to qualitatively assess relative binding affinities when multiple ions of the same species bind. As discussed below, this is straightforward for Cu^{2+} binding, but more difficult for Mn^{2+} binding.

The general procedure employed to locate the sites of metal binding on *B. subtilis* Spo0F involved analyzing the ^{1}H–^{15}N HSQC spectra during the course of the titration and mapping significant diamagnetic metal-induced chemical shift perturbations or paramagnetic metal-induced line broadening onto the previously solved structure of Spo0F (Madhusudan *et al*. 1997). Summaries of the titrations involving diamagnetic (Mg^{2+} and Ca^{2+}) and paramagnetic (Mn^{2+} and Cu^{2+}) metals are found in Figures 2 and 4, respectively, and include graphical and structural plots of the most significantly affected residues, as well as trends in the form of bar graphs for all residues followed during the respective titrations.

Results from the Mg^{2+} titration of *B. subtilis* Spo0F are shown in Figure 2a–c and primarily reveal chemical shift perturbations concentrated around the Asp pocket. Figure 2a shows titration curves for residues most significantly affected ($\Delta\delta_{min} > 0.2$ ppm) as a result of Mg^{2+} titration, which were subsequently plotted onto the structure of *B. subtilis* Spo0F shown in Figure 2b. Chemical shift differences between the beginning and endpoints of the Mg^{2+} titration for all residues followed are shown in Figure 2c. D11, Y13 and M55 are residues that compose or are near the Asp pocket (Figure 2b). Curves from these residues are consistent with the previously measured equilibrium dissociation constant for Mg^{2+} binding, $K_d = 20 \pm 5$ mM (Feher *et al*. 1995). G36 and M60 are found in mobile loop regions in close proximity to the Asp pocket (Figure 2b). Titration curves from these residues (G36 and M60) are similar in shape to the aforementioned residues (D11, Y13 and M55), all of which exhibit the largest changes in chemical shift upon titration of Mg^{2+}. Residues E86, L87, Q91, E92, Y106 and E110 are located the β4-α4 loop and α4/β5/α5 interface and surrounding loop regions (Figure 2b). The titration curves for these residues show an unsaturating effect that occurs at concentrations higher than the previously determined K_d for Mg^{2+}. The shapes of these titration curves (Figure 2a) suggest a slightly more complex

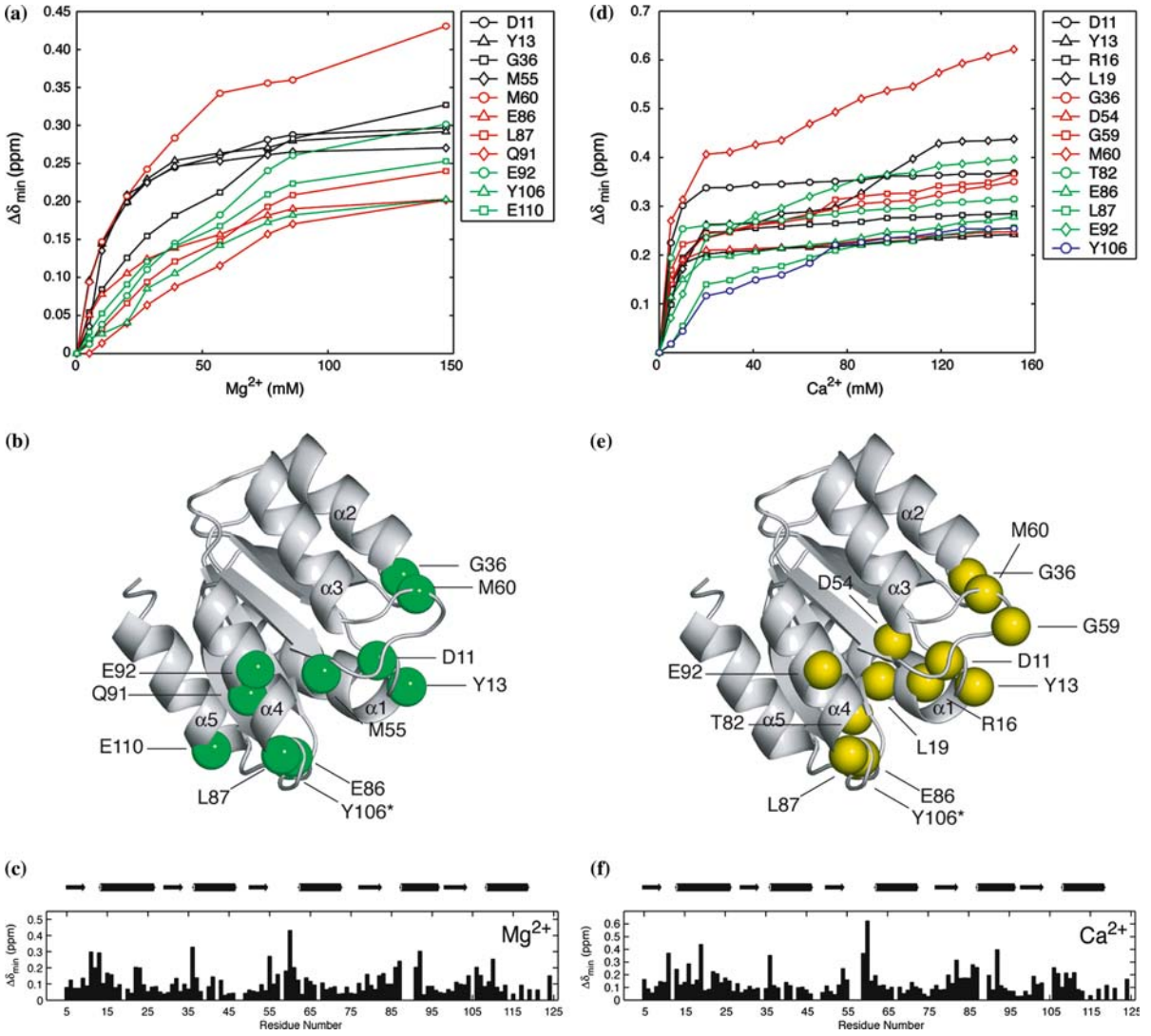

Figure 2. Locations of diamagnetic metal-induced perturbations to *B. subtilis* Spo0F followed using ^{1}H–^{15}N HSQC NMR. Results for the (a–c) Mg^{2+} and (d–f) Ca^{2+} titrations are as follows. Graphical representations of largest chemical shift perturbations for (a) Mg^{2+} and (d) Ca^{2+}. Residues perturbed by (b) Mg^{2+} and (e) Ca^{2+} binding and corresponding to those shown in the graphical representations plotted on the ribbon structure of Spo0F (PDB: 1NAT). Minimum chemical shift differences values for all residues followed in the (c) Mg^{2+} and (f) Ca^{2+} titrations calculated between the beginning and endpoints.

binding response, such as the binding of two metal ions with different affinities. This second metal interaction appears to occur at the residues previously noted in the α4/β5/α5 interface (E86, L87, Q91, E92, Y106 and E110). These data corroborate the results from our previous study of *B. subtilis* Spo0F Mg^{2+}-binding monitored by ^{1}H–^{15}N HSQC, where similar metal ion-induced chemical shift changes were observed in the β4-α4 loop and α4/β5/α5 interface (Feher *et al.* 1995). Because of the concentrations required to elicit the structural change, the secondary binding site around the β4-α4 loop and α4/β5/α5 interface is extremely unlikely to be populated at *in vivo* concentrations of Mg^{2+}. Previously we suggested that this site may bind a different metal cation (Feher *et al.* 1995).

Results from the Ca^{2+} titration of *B. subtilis* Spo0F are shown in Figure 2d–f and reveal trends comparable to those seen in the Mg^{2+} titration. Figure 2d shows titration curves for residues most significantly affected ($\Delta\delta_{min} > 0.23$ ppm) as a result of Ca^{2+} titration, which were subsequently

plotted onto the structure of *B. subtilis* Spo0F shown in Figure 2e. Chemical shift differences between the beginning and endpoints of the Ca^{2+} titration for all residues followed are shown in Figure 2f. D11, Y13, D54 and T82, are residues that compose or are near the Asp pocket (Figure 2e). The Ca^{2+} titration curve for D11, a residue in the Asp pocket, corroborates previous studies that demonstrate Spo0F has a higher affinity for Ca^{2+} compared to Mg^{2+}, 2.5 mM vs. 20 mM, respectively (Mukhopadhyay *et al*. 2004). The Ca^{2+} D11 curve is notably steeper than the curve for the Mg^{2+} D11 curve and reaches saturation faster (Figure 3). R16, G36, G59, M60 are residues found in loop regions or helices close to the Asp pocket (Figure 2e). Titration curves from these residues (R16, G36, G59, M60) are similar to the aforementioned residues (D11, Y13, D54 and T82), all of which exhibit the largest changes in chemical shift upon titration of Ca^{2+}. Furthermore, curves from these residues are consistent with the previously measured equilibrium dissociation constant of 3.5 mM for Ca^{2+} (Mukhopadhyay *et al*. 2004). Residues L19, E86, L87, E92 and Y106 are located the β4-α4 loop and α4/β5/α5 interface and surrounding loop regions, with the exception of L19 that is found on α1 (Figure 2e). Similar to the Mg^{2+} titration, the titration curves for these residues suggest a slightly more complex metal binding response, such as the binding of two metal ions with different affinities.

Results from the paramagnetic Mn^{2+} titration of *B. subtilis* Spo0F are shown in Figure 4a–c and reveal characteristics similar to those seen for the diamagnetic metals Mg^{2+} and Ca^{2+}. Figure 4a shows titration curves for residues most significantly affected in terms of slope of decay of peak intensity (see¶2 of the Results section for details) as a result of Mn^{2+} titration, which were subsequently plotted onto the structure of *B. subtilis* Spo0F shown in Figure 4b. Figure 4c shows the average slope of the intensity curves for all residues between the beginning titration point (0 μM) and the 2, 7 and 27 μM Mn^{2+} titration points. Paramagnetic-induced line broadening effects are evident for residues in proximity to the Asp pocket. The most significant line broadening effects arise from residues in or near the Asp pocket (Figure 4a–c). At ~27 μM Mn^{2+} the peaks from the following residues have significantly dropped

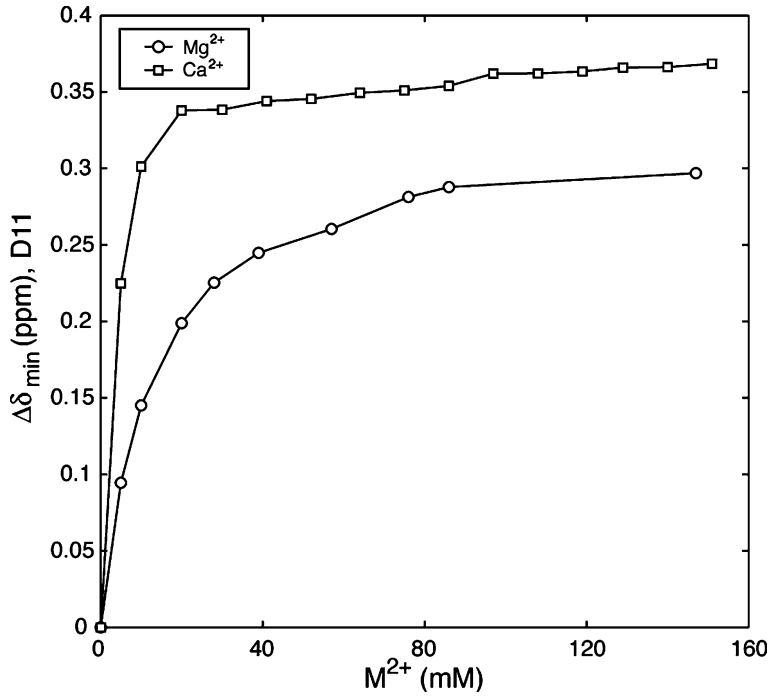

Figure 3. Minimum chemical shift difference titration curves for D11. The titration curves for D11 as a result of Mg^{2+} (circles) or Ca^{2+} (squares) titration is consistent with previous studies detailing the higher affinity of Ca^{2+} for Spo0F compared to Mg^{2+}.

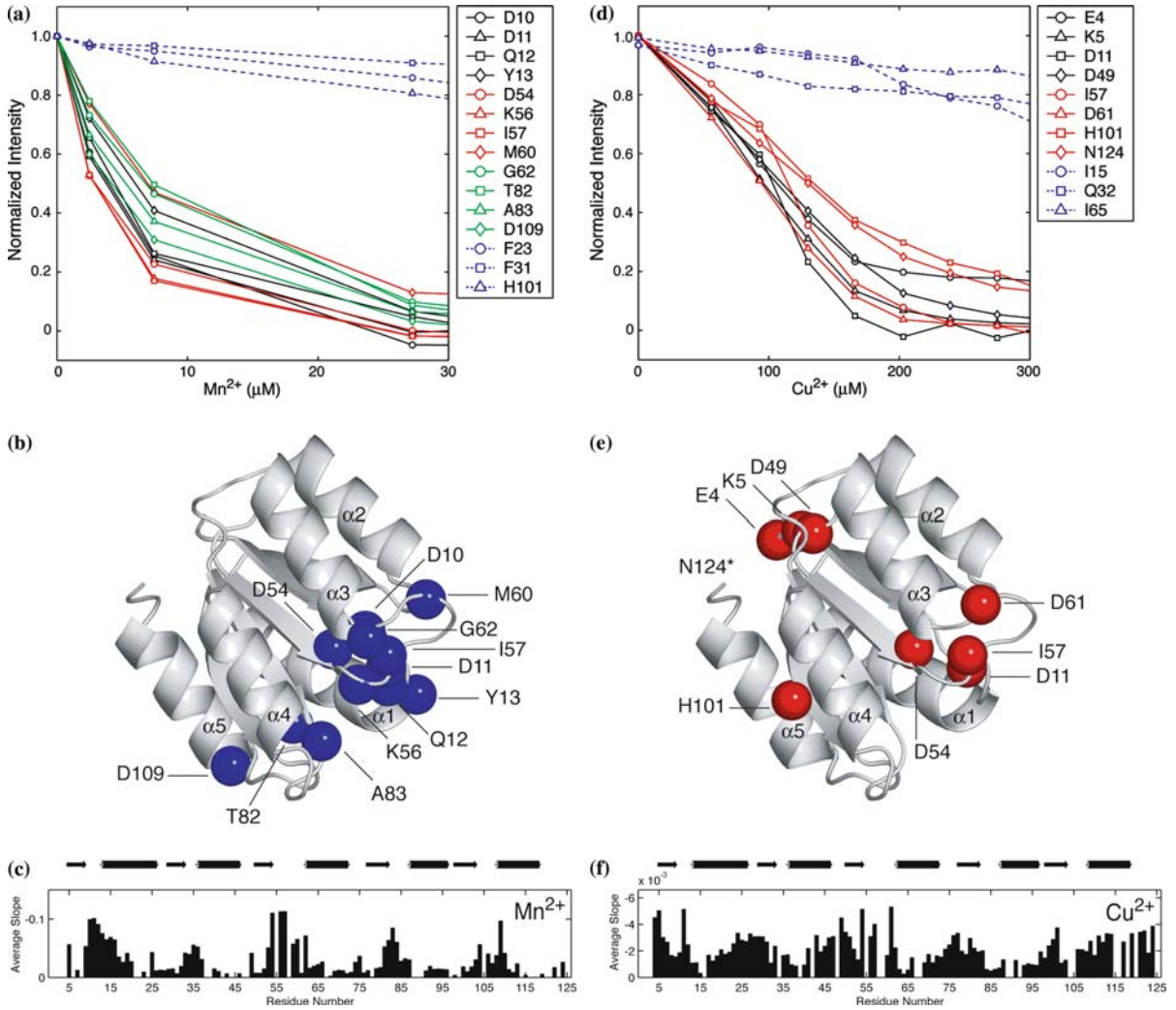

Figure 4. Locations of paramagnetic metal-induced line broadening to *B. subtilis* Spo0F followed using ^{1}H–^{15}N HSQC NMR. Results for the (a–c) Mn^{2+} and (d–f) Cu^{2+} titrations are as follows. Graphical representations of residues most significantly affected as a result of paramagnetic-induced line broadening for (a) Mn^{2+} and (d) Cu^{2+}. Residues affected by (b) Mn^{2+} and (e) Cu^{2+} binding and corresponding to those shown in the graphical representations plotted on the ribbon structure of Spo0F (PDB: 1NAT). Normalized average slope (see Materials and methods) values for all residues followed in the (c) Mn^{2+} and (f) Cu^{2+} titrations calculated between the beginning and endpoints. Residues not observable on the ribbon structure are marked with an asterisk (*).

in intensity and show the largest decrease in peak intensity: D10-Y13, D54, K56, I57, M60, G62, T82 and A83 (Figure 4a, c). In addition, the peak intensity of D109 on α5 interface drops quickly. This again alludes to a secondary binding event in the β4-α4 loop and α4/β5/α5 interface region similar to that seen for Mg^{2+} and Ca^{2+}. As noted above (¶2 of the Results section), the electronic correlation time for Mn^{2+} is relatively long (10^{-8} s). This means that titration curves for many residues are quite steep initially as the paramagnetic effect of the unpaired electron is felt across much of the protein. Thus, it is more difficult to assess the relative affinities of Mn^{2+} binding sites. Consequently, based on the NMR data, we cannot definitively say that the second Mn^{2+} binding event in the β4-α4 loop and α4/β5/α5 interface is weaker than the Mn^{2+} binding in the Asp pocket. A recent crystallographic study of *B. subtilis* Spo0F in the presence of Mn^{2+} revealed a single metal ion bound in the Asp pocket (Mukhopadhyay *et al.* 2004), suggesting that the Mn^{2+} binding event in the Asp pocket is preferential to interaction with the β4-α4 loop and α4/β5/α5

interface region. As a note, addition of paramagnetic metal ions, such as Mn^{2+}, did not cause line broadening of all surface exposed residues. Residues distant from the Asp pocket, e.g. F23 (approx. 19 Å), F31 (approx. 16 Å) and notably H101 (approx. 21 Å), show relatively little change in intensity during the initial points of the titration that affected residues in the Asp pocket (Figure 4c; curves shown in blue with dotted lines). This indicates the effects seen as a result of Mn^{2+} titrations are not a consequence of non-specific binding. Thus far, the results imply that at non-physiological concentrations of metal, Spo0F may have an additional metal binding site at the β4-α4 loop and α4/β5/α5 interface.

Results from the Cu^{2+} titration of *B. subtilis* Spo0F are shown in Figure 4d–f and exhibit a titration profile different than that of the other metals ions studied. Figure 4d shows titration curves for residues most significantly affected in terms of slope of decay of peak intensity (see¶2 of the Results section for details) as a result of Cu^{2+} titration, which were subsequently plotted onto the structure of *B. subtilis* Spo0F shown in Figure 4e. Figure 4f shows the average slope of the intensity curves for all residues between the beginning titration point (0 μM) and the 56, 93, 130 and 166 μM Cu^{2+} titration points. At $\sim$233 μM Cu^{2+}, residues on three surface regions have significantly dropped in intensity and include (i) the Asp pocket (D11, D54, I57, D61), (ii) a grouping of charged residues (E4, K5, D49), and (iii) the β5/α5 interface, particularly around and including H101 (Figure 4e, f).

As in the previous Ca^{2+}, Mg^{2+} and Mn^{2+} titrations, residues in or near the Asp pocket experience paramagnetic-induced line broadening effect as a result of Cu^{2+} titration. However, the Cu^{2+} titration data differs from the other studies as two additional surface regions on *B. subtilis* Spo0F are affected at approximately the same titration point as the Asp pocket. The grouping of charged residues (E4, K5, D49) showing a significant decrease in peak intensity (Figure 4d) is located opposite the Asp pocket (Figure 4e). Other residues, including L50, I76 and R77, which are structurally close to E4, K5 and D49 also exhibit a moderate decrease in intensity (Figure 4f). The third site of interaction is again in the β5/α5 interface, but in this case particularly centered around H101 (Figure 4e). H101 displays a substantial reduction in peak intensity, while residues including T100 and others on α5 display moderate effects as well (Figure 4f). Similar to the Mn^{2+} titration, some residues, including I15, Q32 and I65, display relatively little change in intensity during the titration (Figure 4f), indicating the effects seen as a result of titration of Cu^{2+} are not a consequence of non-specific binding.

Metal binding to B. subtilis Spo0F studied by μESI-MS

μESI-MS (Loo 1997; Cavanagh *et al.* 2003) was used to verify the Spo0F-metal ion binding trends observed in the ^{1}H–^{15}N HSQC NMR experiments. Shown in Figure 5 are the μESI-MS results of concentration-based experiments of four divalent metals studied: Mg^{2+}, Ca^{2+}, Mn^{2+} and Cu^{2+} at metal concentrations of 0, 125, 250 and 375 μM. The monovalent K^{+} and trivalent Mn^{3+} metals were found to not specifically bind to Spo0F to any significant degree (data not shown). This result was not surprising since response regulators are known to specifically bind divalent metals in the Asp pocket.

The divalent ions Ca^{2+}, Mg^{2+} and Mn^{2+} bind to Spo0F in what might be considered a conventional binding mode, where Spo0F preferentially binds a single metal ion. The profile for the Mg^{2+} titration (Figure 5a–d) shows that apo-Spo0F is favored, or possesses the largest relative abundance. Metal-bound peaks in the Mg^{2+} titration are not well resolved, at least compared to the other metals studied, and is likely due the relatively low molecular weight of magnesium compared to the other metals studied. In any case, a $1Mg^{2+}$-Spo0F complex peak begins to appear around the 125 μM titration point (Figure 5b) and becomes somewhat more intense in abundance as the Mg^{2+} concentration is increased. A weak $2Mg^{2+}$-Spo0F complex is slightly observable at the 375 μM titration point (Figure 5d). Additionally, a subset of low abundance peaks corresponding to ^{14}N-labeled Spo0F is observed due to inefficient ^{15}N labeling (see legend of Figure 5).

Figure 5. Spo0F–metal complexes analyzed using μESI-MS. Metal concentration-based titrations of Spo0F (6 μM) in the presence of increasing concentrations of (a–d) Mg^{2+}, (e–h) Ca^{2+}, (i–l) Mn^{2+} and (m–p) Cu^{2+}. The majority of protein complexes observed are from ^{15}N-Spo0F, while low relative ion abundance peaks are observed for ^{14}N-Spo0F (marked with *).

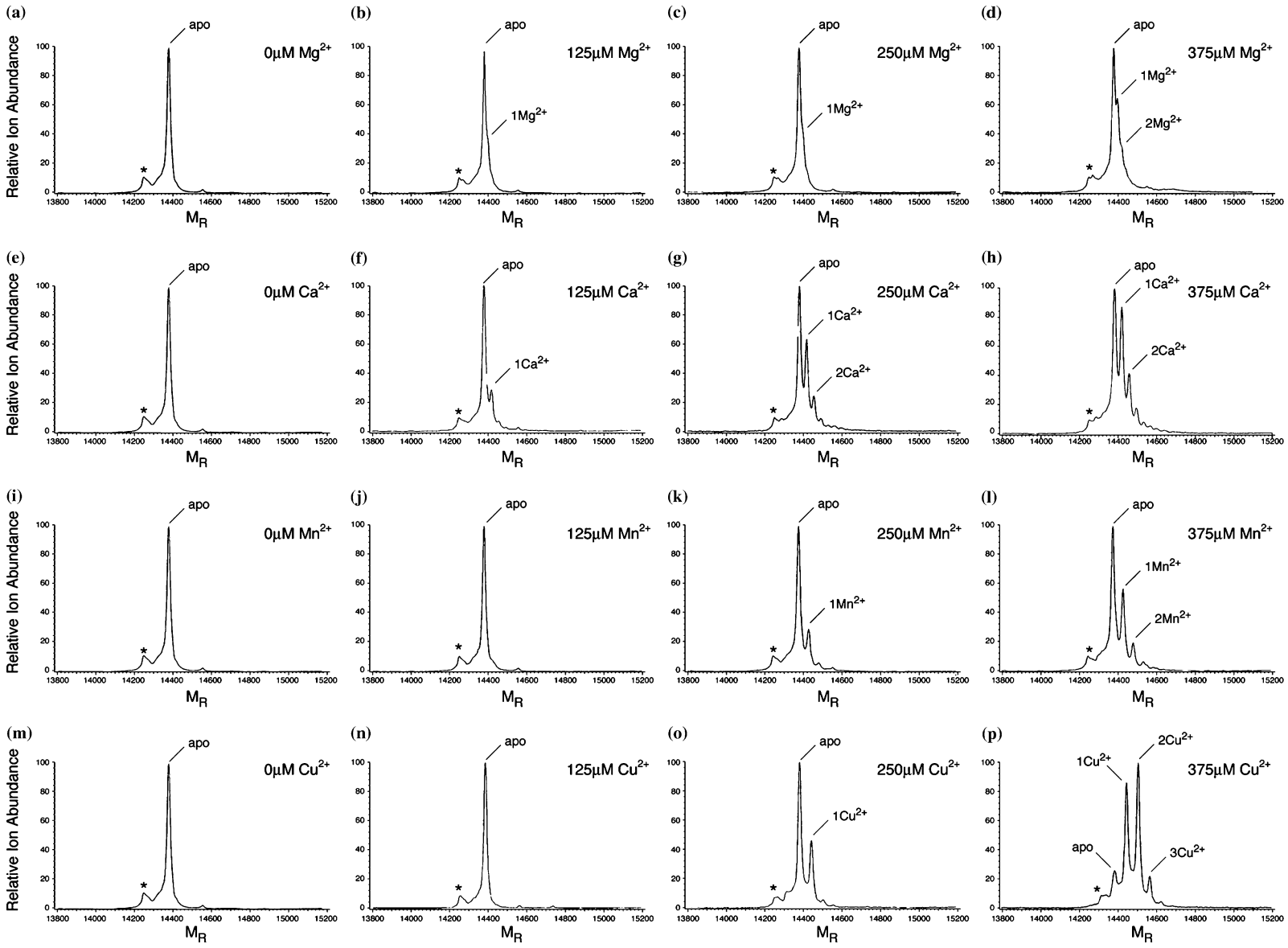
(a)
0μM Mg2+
apo
(b)
125μM Mg2+
apo
1Mg2+
(c)
250μM Mg2+
apo
1Mg2+
(d)
375μM Mg2+
apo
1Mg2+
2Mg2+
(e)
0μM Ca2+
apo
(f)
125μM Ca2+
apo
1Ca2+
(g)
250μM Ca2+
apo
1Ca2+
2Ca2+
(h)
375μM Ca2+
apo
1Ca2+
2Ca2+
(i)
0μM Mn2+
apo
(j)
125μM Mn2+
apo
(k)
250μM Mn2+
apo
1Mn2+
(l)
375μM Mn2+
apo
1Mn2+
2Mn2+
(m)
0μM Cu2+
apo
(n)
125μM Cu2+
apo
(o)
250μM Cu2+
apo
1Cu2+
(p)
375μM Cu2+
apo
1Cu2+
2Cu2+
3Cu2+
Relative Ion Abundance
MR
13800 14000 14200 14400 14600 14800 15000 15200
0 20 40 60 80 100

The profile for the Ca^{2+} titration (Figure 5e–h) shows the $1Ca^{2+}$-Spo0F complex increasing in abundance and to nearly the same intensity as that of the apo-Spo0F complex by the 375 μM titration point (Figure 5h). A two-bound complex becomes observable between the 250 and 375 μM titration points (Figure 5g, h). The profile for the Mn^{2+} titration (Figure 5i–l) shows that apo-Spo0F is favored, with a $1Mn^{2+}$-Spo0F complex increasing to approximately 60% relative abundance. By the 375 μM titration point, a weakly detectable $2Mn^{2+}$-Spo0F complex appears (Figure 5l). At concentrations higher than 375 μM, the $1M^{2+}$-Spo0F complex in each of the three aforementioned titrations increases towards 100% relative abundance, while the $2M^{2+}$-Spo0F complex slightly increases as well (data not shown). Overall, these data suggest that, in terms of stoichiometry, Mg^{2+}, Ca^{2+} and Mn^{2+} bind similarly to Spo0F.

In contrast to the results observed for the previous divalent metals, Cu^{2+} reveals a different binding profile. The profile for the Cu^{2+} titration (Figure 5m–p) shows a $1Cu^{2+}$-Spo0F complex increasing in relative abundance. Unlike the other titrations, where the apo-Spo0F peak is the most intense metal-bound complex between the 250 and 375 μM titration points, the metal-bound complexes in the Cu^{2+} titration have a higher relative abundance (Figure 5p). By the 375 μM titration point, the relative abundance of the $2Cu^{2+}$-Spo0F becomes the most intense complex observed. Additionally, a slightly observable $3Cu^{2+}$-Spo0F complex appears at the 375 μM titration point. At concentrations higher than 375 μM, the relative abundance of the $3Cu^{2+}$-Spo0F complex increases, eventually surpassing the relative abundance for the $2Cu^{2+}$-Spo0F complex (data not shown).

Effect of Mg^{2+} and Cu^{2+} on phosphotransfer between KinA∼P and Spo0F in B. subtilis

To investigate functional consequences of metal binding to Spo0F, with respect to the interaction with its cognate kinase KinA, we examined the effect of two metals with very different binding profiles. The phosphotransfer efficiency between KinA∼P and Spo0F in the presence of Mg^{2+} or Cu^{2+} was investigated (Figure 6). Figure 6a shows that the addition of Mg^{2+} promotes transfer of the phosphoryl group from KinA∼P to Spo0F. The amount of Spo0F∼P is seen to increase as a function of decreasing KinA∼P, which is consistent with previous studies (Zapf *et al*. 1996). There is a negligible drop in Spo0F∼P

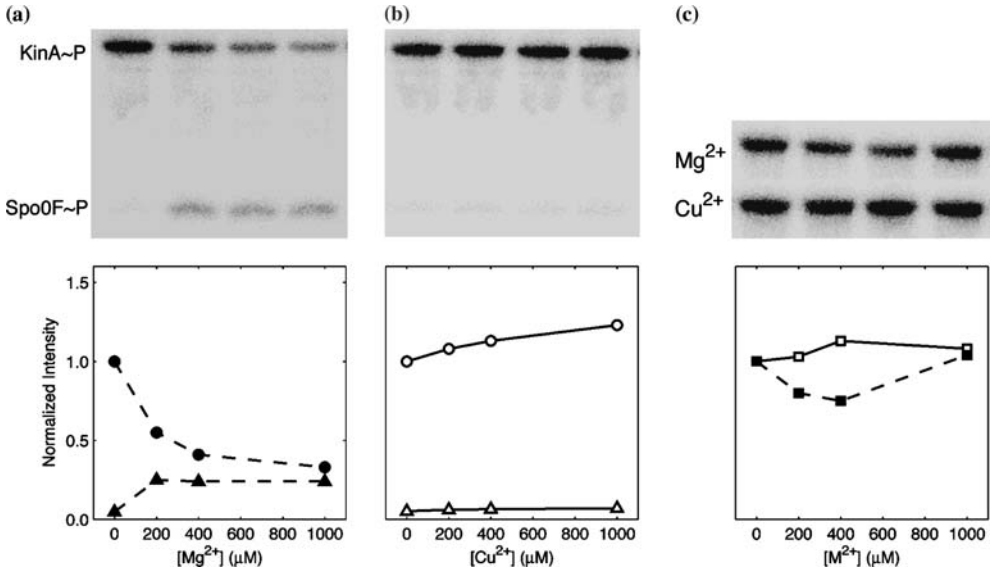

Figure 6. Metal dependence on phosphotransfer between KinA∼P and Spo0F and stability of KinA∼P in *B. subtilis*. (a, b) Phosphotransfer reactions were performed in the presence of increasing concentrations of (a) Mg^{2+} and (b) Cu^{2+}. The presence of Cu^{2+} fails to support phosphotransfer between KinA∼P (circles; filled and unfilled) and Spo0F (triangles; filled and unfilled). (c) KinA∼P is stable in the presence of Mg^{2+} (filled squares) and Cu^{2+} (unfilled squares).

at higher Mg^{2+}, which is likely a result of inefficiency in phosphotransfer, as well as an inherent autophosphatase activity that is present in response regulators (Zapf *et al*. 1998). Figure 6b shows that the addition of Cu^{2+} fails to support this phosphotransfer event between KinA∼P and Spo0F. KinA∼P is stable in the presence of both Mg^{2+} and Cu^{2+} (Figure 6c), suggesting the lack of Spo0F∼P produced is likely a consequence of metal binding to Spo0F rather than a metal-dependent dephosphorylation of KinA∼P.

Effect of copper on spore formation in B. subtilis and P. penetrans

To qualitatively investigate any consequences of copper on *B. subtilis* spore formation, we cultured *B. subtilis* on sporulation media containing increasing amounts of Cu^{2+} and compared the spore formation to a plate containing no Cu^{2+} (Table 1). In the absence of Cu^{2+}, *B. subtilis* cells grew vegetatively and were able to form spores (experiment 0). At low, non-lethal concentrations of Cu^{2+}, spore formation appeared to be inhibited while allowing for vegetative growth (experiments 1 and 2). Higher concentrations of Cu^{2+} had a negative effect on cell growth and subsequently did not allow for vegetative growth and could not produce spores (experiments 3–7).

Recent genetic and phylogenetic analyses of the Gram-positive endospore-producing bacterium *P. penetrans* revealed significant homology with members of the *Bacillus* spp. Preliminary analysis of the partial *P. penetrans* genome has identified homologues to many of the *B. subtilis* sporulation genes (Bird *et al*. 2003), including the genes encoding the following proteins: KinA-E, Spo0A, Spo0B and Spo0F (Opperman, C., unpublished results). A sequence comparison of Spo0F from *B. subtilis* and *P. penetrans* shows them to be 84% similar (Figure 7a), with both possessing the histidine on β5, H101 with respect to *B. subtilis* Spo0F (Figure 7b, c).

To extend our *B. subtilis* studies, we performed a *P. penetrans* sporulation assay in the presence and absence of Cu^{2+} in the growth medium. The results of these studies are shown in Figure 8. When Cu^{2+} is present at 3.89 mM (Figure 8a), endospore formation is slight with the majority of cells present as vegetative rods (inset of Figure 8a). When Cu^{2+} is absent (Figure 8b), an abundance of sporulating cells are visible (inset of Figure 8b) with almost no vegetative cells present. The small white and grey circles, which are particularly noticeable in the experiments in the presence of Cu^{2+} in Figure 8a, are particle in the medium. Overall, we observed approximately a 100-fold decrease in endospore formation in the presence of Cu^{2+}. We also studied the effects of varying the composition of the *P. penetrans* growth and sporulation media (Table 2). We observed that removal of the Cu^{2+} and EDTA, normally found in the standard growth medium of *P. penetrans*, has a positive effect on cell growth and spore formation. Removal of another metal normally found in the media, Zn^{2+}, had no effect on cell growth or spore formation.

Discussion

The complementary NMR and μESI-MS studies presented here show that Mg^{2+}, Ca^{2+} and Mn^{2+}, all show similar binding profiles where the dominant binding event involves a single metal ion. The ^{1}H–^{15}N HSQC NMR titration data for these metals shows that metal ion binding occurs in the Asp pocket, a region of Spo0F that is well known to be affected by metal binding (Feher *et al*. 1995). At higher concentrations, a secondary binding event is also observed near the β4-α4 loop and α4/β5/α5 interface. This binding appears to be specific in nature, since the binding effects monitored by ^{1}H–^{15}N HSQC NMR (Figures 2c, f and 4c, f) do not affect all negatively charged surface patches. For these metals, the μESI-MS studies support the NMR studies in terms of binding stoichiometries, showing a $1M^{2+}$-Spo0F complex as the predominant form and a weakly detectable $2M^{2+}$-Spo0F complex observed at much higher metal ion concentrations. Furthermore, experiments show that in the presence of Mg^{2+}, phosphotransfer between KinA∼P and Spo0F is facilitated. In contrast, the ^{1}H–^{15}N HSQC NMR titration of Cu^{2+} identified three sites of ion binding on Spo0F. This is corroborated by the μESI-MS binding data that shows Spo0F binds up to three ions of Cu^{2+}. Experiments show that the presence of Cu^{2+} fails to support phosphotransfer between KinA∼P and Spo0F. Additional qualitative observations show that, under conditions of non-physiological amounts of Cu^{2+}, *B. subtilis* and *P. penetrans*

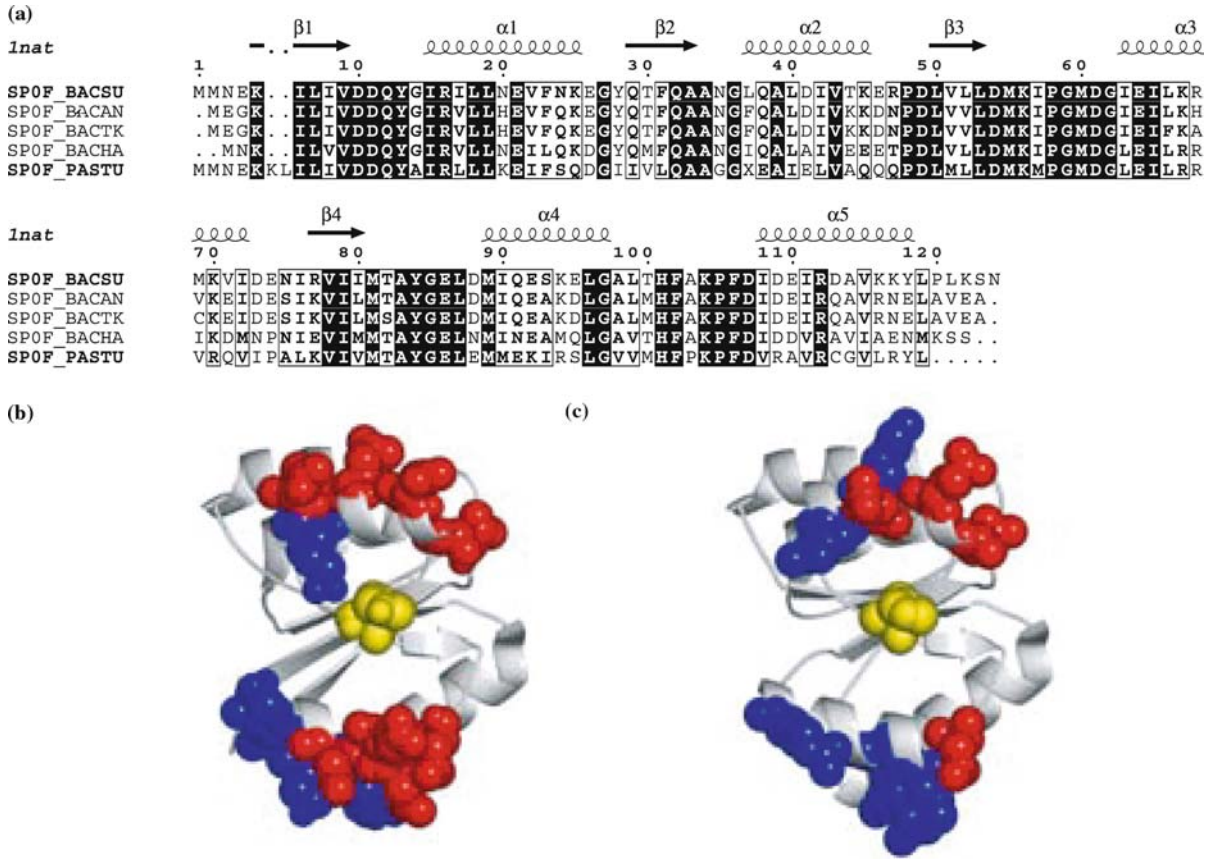

Figure 7. Sequence alignment and surface similarity of Spo0F proteins. (a) Sequences from *Bacillus subtilis* (SP0F_BACSU), *Bacillus anthracis* (SP0F_BACAN), *Bacillus thuringiensis* (SP0F_BACTK), *Bacillus halodurans* (SP0F_BACHA) and *Pasteuria penetrans* (SP0F_PASTU) aligned with secondary structure outlined with reference to Spo0F (PDB: 1NAT). Residues are highlighted as identical/conserved (black box) and similar/conserved (white box). (b, c) Structures models of Spo0F from (b) *B. subtilis* (PDB: 1NAT) and (c) *P. penetrans* (homology model). Residues comprising the $\alpha 4/\beta 5/\alpha 5$ surface are highlighted as follows: yellow (histidine), red (negatively charged), blue (positively charged).

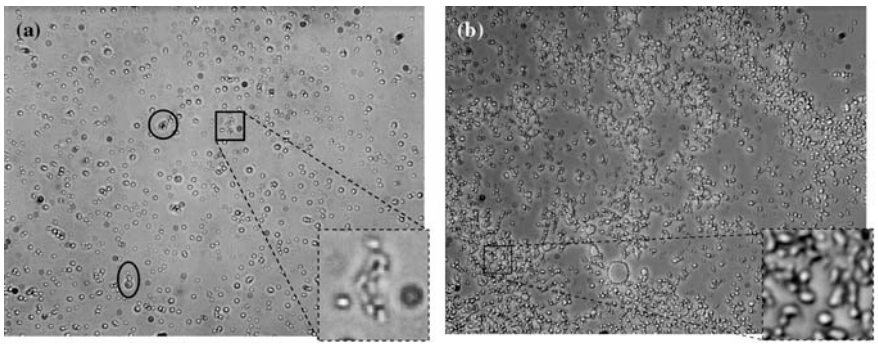

Figure 8. Cu^{2+} dependence of *P. penetrans* endospore formation. Cultures were grown in the (a) presence (3.89 mM) and (b) absence of Cu^{2+}. (a) *P. penetrans* in the presence of Cu^{2+} shows mainly vegetative rods (square; see inset), but other structures such as a microcolony (circle) and a thallose structure (oval), which are capable of producing endospores, are present as well. (b) *P. penetrans* in the absence of Cu^{2+} shows an abundance of sporulating cells (from thalli; see inset), especially concentrated in the lower left quadrant. The small white and gray circles present, particularly noticeable in (a), are particle in the medium.

Table 2. Summary of the effect of copper on *P. penetrans* growth and spore formation.

Experiment	Cell growth	Spore formation
Standard medium	Little	Poor
Without 3.89×10^{-3} M Cu^{2+} and 3.22×10^{-3} M EDTA	Yes	Yes
Without 1.11×10^{-3} M Zn^{2+} and 3.22×10^{-3} M EDTA	Little	Poor
Without 3.89×10^{-3} M Cu^{2+}, 1.11×10^{-3} M Zn^{2+} and 3.22×10^{-3} M EDTA	Yes	Yes

spore formation was not supported. As far as we are aware, other than a study of DivK that revealed a binding site 30 Å from the Asp pocket for $PtCl_4^{2-}$, a component of the crystallization buffer (Gouet *et al.* 1999), our study is unique in the description of a multiple metal binding event for a response regulator.

The slight differences observed in the Cu^{2+} titration profiles (Figure 4d) between residues in the Asp pocket and H101 can be explained by the previously solved structures of *B. subtilis* Spo0F in its apo, M^{2+}-bound and BeF_3-activated forms. These previous studies show that H101 in the apo form of *B. subtilis* Spo0F adopts a buried conformation (Feher *et al.* 1995). In the case of M^{2+}-bound crystal structures, where a single M^{2+} is bound in the Asp pocket, H101 undergoes a conformational change and adopts a more solvent exposed orientation (Madhusudan *et al.* 1996; Mukhopadhyay *et al.* 2004). Furthermore, the BeF_3-activated NMR structure of Spo0F also shows H101 to be solvent exposed (Gardino *et al.* 2003). An illustration of the relative position of H101 in the three aforementioned structural states is shown in Figure 9. In order for a Cu^{2+} sto bind to Spo0F efficiently at H101, a metal ion must first bind in the Asp pocket to elicit a conformational change, resulting in the repositioning of H101 from a buried to a solvent exposed configuration. With respect to our metal binding data, a two-step process can be envisioned where (i) a Cu^{2+} binds first in the Asp pocket forcing H101 more into solution where then (ii) the imidazole ring of H101 is now solvent exposed and can bind the second Cu^{2+}. Without the conformational change at H101 induced by the first Cu^{2+} binding in the Asp pocket, the subsequent Cu^{2+} binding event at H101 could not occur. Titration curves for residues such as D11 and I57, which compose or are in close proximity to the Asp pocket, display Cu^{2+}-induced line broadening effects (larger slopes of decay of peak intensity) slightly *before* the titration curve of H101 (Figure 4d). In terms of the average slope intensity differences (Figure 4f), residues in or near the Asp pocket, display larger slopes of decay of peak intensity when compared to H101 or residues on α5. Cu^{2+} binding to exposed H101 in Spo0F is not surprising since Cu^{2+} binding to single or multiple solvent exposed histidine residues is often exploited during protein purification processes (Sulkowski 1985). It is, therefore, reasonable that the combination of a solvent exposed histidine, such as H101, surrounded by a significant number of negatively charged residues in the α4/β5/α5 region of Spo0F (in both *B. subtilis* and *P. penetrans*; Figure 7) provides an attractive site for Cu^{2+} binding. It is also likely, based on our experiments and previous mutagenesis and structural work, that such an interaction would have an effect on Spo0F function (Feher *et al.* 1995, 1997, 1998; Tzeng & Hoch 1997; Tzeng *et al.* 1998; Feher & Cavanagh 1999; Jiang *et al.* 1999).

Recent studies have suggested that metal ions other than Mg^{2+} may play a role in the regulation of response regulator action, including the initiation of sporulation phosphorelay in *B. subtilis* (Tzeng *et al.* 1998; Mukhopadhyay *et al.* 2004). Mg^{2+} is commonly regarded to as the metal ion of choice for response regulator function. However, a study of Spo0F∼P dephosphorylation by the RapB phosphatase revealed there is likely a preference for a specific metal to perform this function, in this case favoring Mn^{2+} over Mg^{2+} (Tzeng *et al.* 1998). A crystallographic study of Mn^{2+}-bound Spo0F alluded to the possibility of different metals contributing to the control of the complex circuitry of sporulation by affecting phosphotransfer between Spo0F∼P and the phosphotransferase Spo0B (Mukhopadhyay *et al.* 2004). Additionally, a study of the *E. coli* chemotaxis response regulator CheY revealed that Ca^{2+} provided somewhat unfavorable conditions for phosphotransfer and dephosphorylation, whereas all other metal ions studied facilitated these reactions (Lukat *et al.* 1990). Our

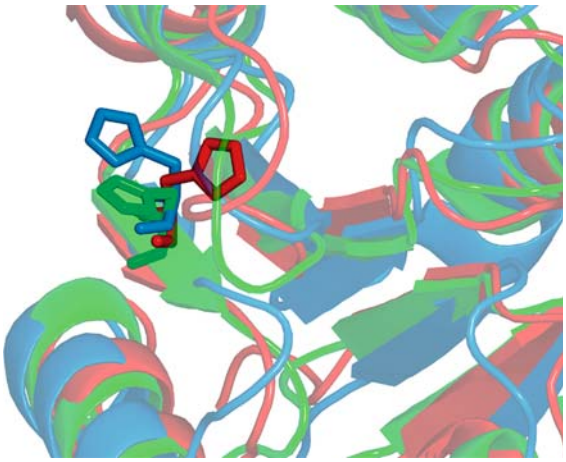

Figure 9. Spo0F structures detail the position of H101 with respect to its active state. Ribbon diagrams of *B. subtilis* Spo0F in the apo (red; PDB: 1FSP), Mn^{2+}-bound (green; PDB: 1PEY) and BeF3-activated (blue; PDB: 1PUX) states. The side chain of H101 is displayed as sticks in the structures to show the transition from a buried to solvent exposed orientation as Spo0F binds metal and becomes activated.

studies suggest that Cu^{2+} could be utilized in the *in vitro* regulation of the sporulation phosphorelay.

NMR studies show that Cu^{2+} not only in binds the Asp pocket but at two other surface locations, one of which includes the highly charged $\alpha4/\beta5/\alpha5$ surface that contains H101 (Figure 7b). There is precedent for effecting response regulator function by means of ligand binding to the $\alpha4/\beta5/\alpha5$ surface of another response regulator, CheY. A drug binding study of CheY identified an inhibitor of the phosphorylation reaction, which was observed by NMR to bind and cause perturbations at the $\alpha4/\beta5/\alpha5$ interface in CheY, a hydrophobic surface that includes the signal residue Y106, which is equivalent to H101 in Spo0F. The binding of this inhibitor is proposed to impact residues important for protein–protein interactions, including interactions between the kinase and response regulator (Hubbard *et al.* 2003). This hydrophobic surface on CheY is the same surface we observe metal binding effects in the Spo0F studies described here. Moreover, the surface regions where these binding effects are observed correlate to the previous mutational studies of *B. subtilis* Spo0F. Mutation of residues in the $\beta4$-$\alpha4$ loop to alanine decrease the V_{max} parameter in kinetic studies between KinA~P and Spo0F (Tzeng & Hoch 1997). Overall, the mutational data in conjunction with our NMR titrations suggests the topology of the $\beta4$-$\alpha4$ loop may play an important role in kinase–Spo0F interactions and perhaps kinase–response regulator interactions in general.

In support of our work, previous studies have detailed the effects of copper on bacterial vegetative growth and sporulation. Early studies reported a requirement, albeit at quite low concentrations, of copper for the sporulation of *B. megateriium* and *B. cereus* (Kolodziej & Slepecky 1962, 1964; Krueger & Kolodziej 1976). In a study of *B. megaterium*, copper uptake was shown to increase somewhat steadily as the sporulation process progressed (Krueger & Kolodziej 1976). This uptake pattern is markedly different from the profiles of other metals (Krueger & Kolodziej 1978). Additional studies have also reported a higher content of copper in *Bacillus* spores when compared to vegetative cells (Curran *et al.* 1943). The observation of increased copper uptake during the progression of sporulation is perhaps not surprising since copper is bound by CotA, an abundant protein of the outer spore coat (Enguita *et al.* 2003). It has also been noted that concentrations of heavy metal ions needed to prevent bacterial growth are usually much lower than those needed to kill bacteria (Kushner 1971). These experiments detailing the copper requirement and uptake patterns during sporulation imply that there are three biochemically important ranges of copper: (i) low concentrations that permit vegetative growth and sporulation, (ii) higher concentrations that inhibit vegetative growth without killing the bacterium, and (iii) even higher concentrations that are lethal as a result of copper toxicity. Our current study suggests there likely exists an additional range, between (i) and (ii), where copper concentrations are such that vegetative growth is allowed yet spore formation is inhibited. Perhaps this is the result of copper interfering with the phosphorelay leading to the initiation of sporulation (Kolodziej & Slepecky 1962; Krueger & Kolodziej 1976). Interestingly, recent studies have shown that *Bacillus* spp. could be useful in the biosorption of Cu^{2+}, with implications of use as a potential biosorbent for copper removal (Lo *et al.* 2003).

It appears that *P. penetrans*, a closely related organism to the *Bacillus* spp., may also be influenced by the presence of Cu^{2+}. Because *P. penetrans* spores are an obligate parasite of root-knot nematodes, which are one of the ten most

destructive pathogens of food crops (Sasser & Freckman 1987), it has been the aim of many researchers to produce mass quantities of *P. penetrans* spores for use as a safe biocontrol agent. Despite the considerable advantages, the ability to mass produce *P. penetrans* spores, the most efficient means of distribution, from an efficient *in vitro* culturing system has proven elusive and has severely hindered efforts to develop this system for nematode biocontrol. However, our present study and others indicate that removal of copper from the commercially developed *Pasteuria* growth/sporulation media provides improved culture conditions for spore formation (Hewlett *et al.* 2002; Gerber *et al.* 2003). These studies previously described suggest that copper could prove useful as a *in vitro* biochemical control in regulating spore formation in other systems, including human pathogenic bacteria such as *B. anthracis* (anthrax) and *B. cereus* (food poisoning).

Conclusions

In summary, comprehensive NMR and μESI-MS studies were performed to investigate the differential binding traits of a variety of divalent metal ions with the sporulation inducing response regulator Spo0F. These studies were combined with a series of metal-based biochemical and sporulation experiments to relate the biophysical data with potential function. Our investigations show that Mg^{2+}, and suggest that metals such as Ca^{2+} and Mn^{2+}, which display primarily 1:1 binding profiles, provide favorable conditions for phosphotransfer from KinA$\sim$P to Spo0F. Conversely, Cu^{2+} was observed to bind to three distinct surface locations and did not facilitate phosphotransfer between KinA$\sim$P and Spo0F.

These studies strongly suggest that the seemingly unique binding properties of Cu^{2+} to *B. subtilis* Spo0F, specifically at $\alpha4/\beta5/\alpha5$ interface, may induce structural effects propagating to the $\beta4$-$\alpha4$ loop. It has been suggested that the topology of the $\beta4$-$\alpha4$ loop is crucial for sensor kinase–response regulator interactions and subsequent phosphorylation to occur (Feher *et al.* 1998; Feher & Cavanagh 1999). This represents a prospective means to stop the progression of sporulation at stage 0. Additionally, our Spo0F Cu^{2+} studies, in combination with the CheY drug binding study, suggests that inhibiting sensor kinase–response regulator interactions through the manipulation of the topology of the $\beta4$-$\alpha4$ loop by means of ligand binding to the $\alpha4/\beta5/\alpha5$ interface may represent a universal site of targeting to response regulators. Furthermore, this work suggests that controlling specific metal ion levels, such as Cu^{2+}, may provide a specific means for biochemical control of spore formation *in vitro*.

Acknowledgements

The authors would like to thank Dr. Kevin Gardner (University of Texas Southwestern Medical Center at Dallas) for kindly providing scripts to analyze the divalent metal ion NMR titration data, Dr. Michael B. Goshe (North Carolina State University) for helpful discussions and Benjamin Bobay (North Carolina State University) for helpful discussions and critical reading of the manuscript. The authors would like to acknowledge support from the following sources: NIH GM55769 (JC), the Kenan Institute for Engineering, Technology and Science (JC), the Mayo Foundation, Rothamsted Research, Ltd., the Lawes Agricultural Trust, North Carolina Agricultural Research Service and Sygenta.

References

Bax A, Ikura M, Kay LE, Torchia DA, Tschudin R. 1990 Comparison of different modes of 2-dimensional reverse-correlation NMR for the study of proteins. *J Magn Reson* **86**, 304–318.

Bertini I, Luchinat C. 1998 Electron-nucleus interactions and their biophysical consequences. Nuclear Magnetic Resonance. D. Gorenstein, Biophysical Society.

Bird DM, Opperman CH, Davies KG. 2003 Interactions between bacteria and plant-parasitic nematodes: now and then. *Int J Parasitol* **33**, 1269–1276.

Burbulys D, Trach KA, Hoch JA. 1991 Initiation of sporulation in *B. subtilis* is controlled by a multicomponent phosphorelay. *Cell* **64**, 545–552.

Cavanagh J, Benson LM, Thompson R, Naylor S. 2003 In line desalting mass spectrometry for the study of noncovalent biological complexes. *Anal Chem* **75**, 2949–2954.

Cavanagh J, Fairbrother WJ, Palmer AGI, Skelton NJ. 1996 Protein NMR Spectroscopy: Principles and Practice. Academic Press; San Diego.

Curran HR, Brunstetter BC, Myers AT. 1943 Spectrochemical analysis of vegetative cells and spores of bacteria. *J Bacteriol* **45**, 485–494.

Delaglio F, Grzesiek S, Vuister GW, Zhu G, Pfeifer J, Bax A. 1995 NMRPipe: a multidimensional spectral processing system based on UNIX pipes. *J Biomol NMR* **6**, 277–293.

Enguita FJ, Martins LO, Henriques AO, Carrondo MA. 2003 Crystal structure of a bacterial endospore coat component. A laccase with enhanced thermostability properties. *J Biol Chem* **278**, 19416–19425.

Farmer BT 2nd, Constantine KL, Goldfarb V, *et al*. 1996 Localizing the $NADP^+$ binding site on the MurB enzyme by NMR. *Nat Struct Biol* **3**, 995–997.

Fawcett P, Eichenberger P, Losick R, Youngman P. 2000 The transcriptional profile of early to middle sporulation in *Bacillus subtilis*. *Proc Natl Acad Sci USA* **97**, 8063–8068.

Feher VA, Cavanagh J. 1999 Millisecond-timescale motions contribute to the function of the bacterial response regulator protein Spo0F. *Nature* **400**, 289–293.

Feher VA, Tzeng YL, Hoch JA, Cavanagh J. 1998 Identification of communication networks in Spo0F: a model for phosphorylation-induced conformational change and implications for activation of multiple domain bacterial response regulators. *FEBS Lett* **425**, 1–6.

Feher VA, Zapf JW, Hoch JA, Dahlquist FW, Whiteley JM, Cavanagh J. 1995 ^1H, ^{15}N, and ^{13}C backbone chemical shift assignments, secondary structure, and magnesium-binding characteristics of the *Bacillus subtilis* response regulator, Spo0F, determined by heteronuclear high-resolution NMR. *Protein Sci* **4**, 1801–1814.

Feher VA, Zapf JW, Hoch JA, *et al*. 1997 High-resolution NMR structure and backbone dynamics of the *Bacillus subtilis* response regulator, Spo0F: implications for phosphorylation and molecular recognition. *Biochemistry* **36**, 10015–10025.

Gardino AK, Volkman BF, Cho HS, Lee SY, Wemmer DE, Kern D. 2003 The NMR solution structure of BeF_3^--activated Spo0F reveals the conformational switch in a phosphorelay system. *J Mol Biol* **331**, 245–254.

Gerber JF, Hewlett TE, Smith KS, White JH. 2003 Materials and methods for *in vitro* production of bacteria. Patent Application Number 20030232422.

Gouet P, Fabry B, Guillet V, *et al*. 1999 Structural transitions in the FixJ receiver domain. *Struct Fold Des* **7**, 1517–1526.

Grimshaw CE, Huang S, Hanstein CG, *et al*. 1998 Synergistic kinetic interactions between components of the phosphorelay controlling sporulation in *Bacillus subtilis*. *Biochemistry* **37**, 1365–1375.

Hewlett TE, Gerber JF, Smith KS, White JH. 2002 *In vitro* culture of *Pasteuria penetrans*. *Fourth International Congress of Nematology, Tenerife*.

Hubbard JA, MacLachlan LK, King GW, Jones JJ, Fosberry AP. 2003 Nuclear magnetic resonance spectroscopy reveals the functional state of the signalling protein CheY in vivo in *Escherichia coli*. *Mol Microbiol* **49**, 1191–1200.

Jiang M, Tzeng YL, Feher VA, Perego M, Hoch JA. 1999 Alanine mutants of the Spo0F response regulator modifying specificity for sensor kinases in sporulation initiation. *Mol Microbiol* **33**, 389–395.

Johnson BA, Blevins RA. 1994 NMRView – a computer-program for the visualization and analysis of NMR data. *J Biomol NMR* **4**, 603–614.

Kolodziej BJ, Slepecky RA. 1962 A copper requirement for the sporulation of *Bacillus megaterium*. *Nature* **194**, 504–505.

Kolodziej BJ, Slepecky RA. 1964 Trace metal requirements for sporulation of *Bacillus megaterium*. *J Bacteriol* **88**, 821–830.

Krueger WB, Kolodziej BJ. 1976 Measurement of cellular copper levels in *Bacillus megaterium* during exponential growth and sporulation. *Microbios* **17**, 141–147.

Krueger WB, Kolodziej BJ. 1978 Divalent cation mobility throughout exponential growth and sporulation of *Bacillus megaterium*. *Microbios* **18**, 159–167.

Kushner, DJ. 1971 *Influence of Solutes and Ions on Microorganisms. Inhibition and Destruction of the Microbial Cell*. W. B. Hugo. London, New York: Academic Press, xiii, 819.

Lo W, Ng LM, Chua H, Yu PH, Sin SN, Wong PK. 2003 Biosorption and desorption of copper (II) ions by *Bacillus* sp. *Appl Biochem Biotechnol* **105–108**, 581–591.

Loo JA. 1997 Studying noncovalent protein complexes by electrospray ionization mass spectrometry. *Mass Spectrom Rev* **16**, 1–23.

Lukat GS, Stock AM, Stock JB. 1990 Divalent metal ion binding to the CheY protein and its significance to phosphotransfer in bacterial chemotaxis. *Biochemistry* **29**, 5436–5442.

Madhusudan M, Zapf J, Hoch JA, Whiteley JM, Xuong NH, Varughese KI. 1997 A response regulatory protein with the site of phosphorylation blocked by an arginine interaction: crystal structure of Spo0F from *Bacillus subtilis*. *Biochemistry* **36**, 12739–12745.

Madhusudan M, Zapf J, Whiteley JM, Hoch JA, Xuong NH, Varughese KI. 1996 Crystal structure of a phosphatase-resistant mutant of sporulation response regulator Spo0F from *Bacillus subtilis*. *Structure* **4**, 679–690.

Mizuno T. 1998 His-Asp phosphotransfer signal transduction. *J Biochem (Tokyo)* **123**, 555–563.

Mukhopadhyay D, Sen U, Zapf J, Varughese KI. 2004 Metals in the sporulation phosphorelay: manganese binding by the response regulator Spo0F. *Acta Crystallogr D Biol Crystallogr* **60**, 638–645.

Sasser JN, Freckman DW. 1987 A world perspective on nematology. In: Dickson, DW, Veech, JA eds. *Vistas on Nematology: A Commemoration of the Twenty-fifth Anniversary of the Society of Nematologists*. Hyattsville, MD: Society of Nematologists; 7–14.

Schaeffer P, Millet J, Aubert JP. 1965 Catabolic repression of bacterial sporulation. *Proc Natl Acad Sci USA* **54**, 704–711.

Sulkowski E. 1985 Purification of proteins by IMAC. *Trends Biotechnol* **3**, 1–11.

Tzeng YL, Feher VA, Cavanagh J, Perego M, Hoch JA. 1998 Characterization of interactions between a two-component response regulator, Spo0F, and its phosphatase, RapB. *Biochemistry* **37**, 16538–16545.

Tzeng YL, Hoch JA. 1997 Molecular recognition in signal transduction: the interaction surfaces of the Spo0F response regulator with its cognate phosphorelay proteins revealed by alanine scanning mutagenesis. *J Mol Biol* **272**, 200–212.

West AH, Stock AM. 2001 Histidine kinases and response regulator proteins in two-component signaling systems. *Trends Biochem Sci* **26**, 369–376.

Zapf JW, Hoch JA, Whiteley JM. 1996 A phosphotransferase activity of the *Bacillus subtilis* sporulation protein Spo0F that employs phosphoramidate substrates. *Biochemistry* **35**, 2926–2933.

Zapf J, Madhusudan M, Grimshaw CE, Hoch JA, Varughese KI, Whiteley JM. 1998 A source of response regulator autophosphatase activity: the critical role of a residue adjacent to the Spo0F autophosphorylation active site. *Biochemistry* **37**, 7725–7732.

Zapf J, Sen U, Madhusudan M, Hoch JA, Varughese KI. 2000 A transient interaction between two phosphorelay proteins trapped in a crystal lattice reveals the mechanism of molecular recognition and phosphotransfer in signal transduction. *Struct Fold Des* **8**, 851–862.